Limitations of synthetic aperture laser optical feedback imaging

Wilfried Glastre, Olivier Jacquin, Olivier Hugon, Hugues Guillet de Chatellus, Eric Lacot

Limitations of synthetic aperture laser optical feedback imaging

Wilfried Glastre*, Olivier Jacquin, Olivier Hugon, Hugues Guillet de Chatellus, and Eric Lacot

Centre National de la Recherche Scientifique / Université de Grenoble 1,

Laboratoire Interdisciplinaire de Physique, UMR 5588,

Grenoble, F- 38041, France

**Corresponding author: wilfried.glastre@ujf-grenoble.fr*

In this paper we study the origin and the effect of amplitude and phase noise on Laser Optical Feedback Imaging (LOFI) associated with Synthetic Aperture (SA) imaging system. Amplitude noise corresponds to photon noise and acts as an additive noise, it can be reduced by increasing the global measurement time. Phase noise can be divided in three families: random, sinusoidal and drift phase noise; we show that it acts as a multiplicative noise. We explain how we can reduce phase noise by making oversampling or multiple measurements depending on its type. This work can easily be extended to all SA systems (Radar, Laser or Terahertz), especially when raw holograms are acquired point by point.

OCIS codes: 070.0070, 090.0090, 110.0113, 180.0180.

1) Introduction

Making images with a good in-depth resolution through scattering media is a major issue, limited by a double problematic. Firstly the scattering medium generally strongly attenuates the ballistic photons signal which enables to obtain resolved images and the wavefront is highly perturbed by scattered photons, degrading the quality of the resolved image. Secondly concerning the accessible depth in samples, we are limited by the working distance of the objective. Regarding the first issue, several ways to overcome these problems have been proposed among which we can distinguish two main families. The first one uses pre-compensation of the wavefront before propagation, to improve the resolution. This technique is successfully used both with optics or acoustic modalities [1,2,3], but it requires an *a priori* knowledge of the medium. The second one selects ballistic photons while rejecting multi-diffused parasitic photons: Optical Coherence Tomography (OCT) [4] and confocal microscopy associated [5] or not [6] to non linear effects belong to this family as well as tomographic diffractive microscopy [7] and Laser Optical Feedback Imaging (LOFI), based on optical reinjection in the laser cavity [8,9]. The principle of this technique is to use a laser both as a source and a detector of photons. By analyzing the coherent interaction between the emitted and reinjected photons, it is possible to know the complex amplitude and phase of the reinjected electric field. Amplitude [10] and/or phase [11] images can be obtained by scanning the object point by point with galvanometric mirrors or mechanical translations. We previously showed [12,13] that LOFI benefits from shot noise-limited sensitivity which makes LOFI an excellent imaging system in strongly scattering media,. Moreover LOFI has the advantage of being self-aligned and is therefore easy to implement. Regarding the solution to the second problem (accessible depth in samples), we have shown in [14] that LOFI opens the way to another possibility: imaging beyond the objective working distance, which is important to make deep images with high resolution. This is possible because

LOFI gives both amplitude and phase information, therefore the blurred raw image from a scan beyond the working distance of the objective can be numerically refocused, keeping its initial numerical aperture. This operation is called Synthetic Aperture (SA). This paper is a continuation of [14] which presented the technique of SA-LOFI. We now consider a more realistic case including noise during raw acquisition and we analyze its effects on the final synthetic images. Parasitic reflections occur on optical elements; we have shown in [15] that they can be divided in two groups: specular or diffusive and that in absence of other noise, specular noise is constant and can be filtered out. As a result, diffusive parasitic reflections are the main limitation. In this paper, we investigate the other sources of noise that can disrupt an acquisition and to simplify this study, we neglect parasitic reflections. More precisely, we first focus on laser quantum noise which is an additive noise. Then, we explore phase noise which can be divided in three families: random, sinusoidal and drift phase noises and which acts as a multiplicative noise. We identify their sources, assess their level and their consequences and propose several ways to handle them.

2) Reminder on our previous setup [14]

Experimental setup

Our study is based on the LOFI experimental setup [14] and it is shown on Figure 1. The laser source is highly sensitive to reinjected photons scattered by the target to be imaged. Both amplitude and phase of the reinjected electric field are accessible.

Figure 1 here

The image is obtained point by point by a 2D scanning of the two galvanometric mirrors M_X and M_Y. The use of galvanometric mirrors enables to limit parasitic vibrations (leading to phase noise

in the signal) and to make fast acquisition compared to mechanical translational scanning. However, vibrations can not be totally eliminated and their consequences are developed later in this paper. These mirrors are conjugated in the focal object plane of L_4 and as a result when the mirrors are rotating, the beam scans the target with a translational movement. The scanning is made fast along one direction (X direction) and slowly along Y direction so the acquisition is made point by point and line by line.

The goal of our setup is to get resolved images beyond the classical working distance of the lens (or objective) L_4. The target is placed at a distance L after the image focal plane of L_4 (Figure 1). Without any numerical treatment, by simply scanning the object in this configuration, we only get a raw complex defocused image. However we showed in [14] that using an appropriate numerical filtering, it is possible to refocus this raw image into a resolved image with the same resolution we would have if the object were in the image focal plane of L_4 (given by the beam waist $r/\sqrt{2}$). It is equivalent to say that we are able to artificially increase the working distance of L_4 while keeping its numerical aperture constant, at the price of a degradation of the photometric balance [14]. This numerical treatment applied to raw images is Synthetic Aperture (SA) operation which is possible because we have both amplitude and phase information.

Raw Point Spread Function (PSF)

We showed in [14] that in paraxial and far field conditions and with perfectly aligned optics, the raw signal of a punctual target is:

$$h_R(L,x,y) \propto \left| \exp\left(-\frac{x^2+y^2}{2\,RES_R^{\,2}}\right) \exp\left(j\pi \frac{x^2+y^2}{2\frac{L}{2}\lambda}\right) \right|^2$$
$$RES_R = \frac{\lambda L}{\pi\sqrt{2}r} \qquad (1)$$

This corresponds to a wavefront of lateral spatial width $RES_R(L)$ and a radius of curvature L / 2. The Fourier transform of $h_R(L,x,y)$ is given by:

$$H_R(\nu,\mu) \propto \exp\left(-\frac{\upsilon^2+\mu^2}{\Delta\upsilon^2}\right) \exp\left(-j\frac{\pi L\lambda(\nu^2+\mu^2)}{2}\right)$$
$$\Delta\upsilon = \frac{\sqrt{2}}{\pi r} \qquad (2)$$

In this expression (υ,μ) are the spatial frequencies associated with (x,y) and Δυ is the spectral width of the raw signal.

Point Spread Function after Synthetic Aperture operation

Because the raw signal corresponds to a wavefront defocused over a distance L / 2, we can recover the resolution by simply filtering the raw signal with $H_{filt}(L,\upsilon,\mu)$ the free space transfer function over a distance – L / 2. We shown is [14] that the final synthetic signal is given by:

$$\left|h_{SA}(x,y)\right| = \left|FT^{-1}(H_R(\upsilon,\mu)H_{filt}(\upsilon,\mu))\right| \propto \exp\left(-\frac{x^2+y^2}{RES_{SA}^{\,2}}\right)$$
$$RES_{SA} = \frac{r}{\sqrt{2}} \qquad (3)$$

with FT^{-1} the inverse Fourier Transform operation:

$$H_{\text{filt}}(\nu,\mu) = \exp\left(\ j\frac{\pi L\lambda(\nu^2+\mu^2)}{2}\right) \quad (4)$$

We finally recover a resolution $RES_{SA} \sim r$ whatever the initial defocus is (*i.e.* L). In the following we study the effects on the final synthetic images of amplitude and phase noises. For the need of our demonstrations, we use the object shown on Figure 2.

Figure 2 here

3) Additive noise

Because of the LOFI sensitivity [12,13], this noise is mainly due to the laser quantum noise and the detection is limited by the detection of one photon during the pixel integration time T.

Problems and solutions to amplitude noise: theoretical analysis

We show here that there are two main ways to reduce amplitude noise: increase of the pixel integration time T or spatial oversampling of the initial raw image (causing an increase of the number of pixels N_{pix}). These two methods both increase the Signal to Noise Ratio (SNR) proportionally to the total acquisition time T_{Tot}:

$$T_{Tot} = N_{pix}\,T \quad (5)$$

We now detail the two methods.

Increase of the integration time

Here we show that an increase of the integration time T while keeping the pixel number constant decreases the shot noise level. The signal power (the square of the signal proportional to the flux of reinjected photons) does not depend on T whereas the noise power (proportional to the

variance of the signal) is inversely proportional to T. Then the SNR (signal to noise ratio in energy) is proportional to T. Because N_{pix} is constant here, we get from Eq. (5):

$$SNR \propto T \propto T_{Tot} \tag{6}$$

Oversampling of the raw image

We now focus on a second way to reduce the influence of the additive noise: increase the number of pixels while the pixel integration time is kept constant. The random additive noise in the Fourier space spreads on the whole spectrum. This total spectrum is directly related to the sampling width with $2\Delta\upsilon_{Sh} = 1 / \delta x$ (size of total spatial spectral field recorded in direction X), where δx is the distance between two pixels in the X direction. Assuming that the sampling is the same in the X and Y directions, the surface of this Fourier noise spectrum is given by $S_{NSpect} = 4\Delta\upsilon_{Sh}^2 = 1 / \delta x^2$. However we can see from Eq. (2) and Figure 3, that the signal is localized over a surface (in the power spectral field) $S_{SSpect} = \pi\Delta\upsilon^2/2$ (the factor 2 is because we consider the Fourier power). As a result, it is possible to improve the final SNR by using an amplitude and phase filtering, instead of a pure phase filtering like in Eq. (4). Then the major part of the signal information is preserved (only a factor 2 is lost corresponding to extreme plane waves) while most of the noise is rejected. This type of filter has already been used in SA-LOFI but in a rotational configuration [15,16]. If we want to optimize the SNR, the most appropriate filter is called the adapted filter (well known in Radar temporal field) and is given by $H'_{Filt}(\upsilon,\mu)$:

$$H'_{Filt}(\nu,\mu) = \exp\left(-\frac{\upsilon^2+\mu^2}{\Delta\upsilon^2}\right)\exp\left(j\frac{\pi L\lambda(\nu^2+\mu^2)}{2}\right) \tag{7}$$

This filtering leads to the following synthetic signal:

$$\left|h'_{SA}(x,y)\right| = \left|TF^{-1}(H_R(x,y)H_{filt}(x,y))\right| \propto \exp(-\frac{x^2+y^2}{r^2}) \quad (8)$$

By comparing with Eq. (3), we can see that the improvement of the photometric performances with this filter for is obtained at the cost of a lower resolution by a factor √2. This comes from the fact that extreme plane waves in the signal are lost. More precisely, concerning the photometric performances, the use of this filter turns S_{NSpect} and S_{SSpect} into $S'_{NSpect} = \frac{\pi\Delta\upsilon^2}{2} = \frac{\pi\Delta\upsilon^2}{8\Delta\upsilon_{Sh}^2} S_{NSpect}$ and $S'_{SSpect} = S_{SSpect}/2$. We finally get an improvement in the SNR given by:

$$\frac{SNR_{AdaptFilt}}{SNR_{PhFilt}} = \frac{\frac{S'_{SSpect}}{S'_{NSpect}}}{\frac{S_{SSpect}}{S_{NSpect}}} = \frac{S'_{SSpect}}{S_{SSpect}}\frac{S_{NSpect}}{S'_{NSpect}} = \frac{1}{2}\frac{8\Delta\upsilon_{Sh}^2}{\pi\Delta\upsilon^2} = \frac{1}{\pi\Delta\upsilon^2\delta x^2} \propto N_{Pix} \quad (9)$$

In this expression $SNR_{AdaptFilt}$ and SNR_{PhFilt} are respectively the SNR with and without adapted filter. Because of the constant integration time T for each pixel, the total measurement time is proportional to the spatial sampling and Eq. (9) can be written:

$$\frac{SNR_{AdaptFilt}}{SNR_{PhFilt}} \propto N_{pix} \propto T_{Tot} \quad (10)$$

Then whatever the method used to improve the SNR is, the latter is directly proportional to the total measurement time T_{Tot}.

Experimental results

We now illustrate the theoretical predictions with simulated and experimental data. We show on Figure 3 the Fourier transform amplitudes of a simulated PSF for different spatial samplings (Eq. (2)).

Figure 3 here

Figure 3 shows that the higher the sampling rate is, the stronger the signal isolation is in the total spectrum and consequently proves the possibility to filter additive noise. We now show on Figure 4 the effect of the oversampling and of the use of adapted filtering on a real image of the object of Figure 2.

Figure 4 here

Figure 4 shows that the adapted filtering of an oversampled acquisition is a good way to improve the SNR. On Figure 5, we measure the evolution of the power (square of the amplitude normalized by the number of pixels) of both signal and noise when increasing the integration time (Figure 5a) or the pixel number combined with adapted filtering (Figure 5b).

Figure 5 here

Figure 5 illustrates the fact that when the total measurement time T_{Tot} is increased (by increasing T or N_{pix}), the signal power remains unchanged while the noise is reduced proportionally to T_{Tot} ,which validates the theoretical predictions of the previous section. Note that the signal power is divided by a factor 2 when adapted filtering is used (Figure 5b) which is conform to the theory. To conclude this section it remains preferable to increase the integration time instead of oversampling the signal, which slightly degrades the resolution.

4) Imperfections in phase acquisition (multiplicative noise)

In this section, we analyse the effect of phase noise on a raw acquisition. Because it is a multiplicative noise, it impacts final synthetic images very differently: instead of being simply added to the ideal image it turns a part of the signal power into parasitic noise, depending on the nature of the phase noise. Here, we study the three main phase perturbations we meet: random phase noise, sinusoidal phase noise and phase drifts. Reminding that the raw acquisition of Eq. (1) is the expression of a wavefront of lateral spatial width $RES_R(L)$ and a radius of curvature L / 2, we make analogies with well known physical situations to simplify our analysis and avoid tedious calculations.

Random phase noise

Phase noise has several origins: random mechanical movements (ground, table, galvanometric mirrors) or lack of perfect repeatability in position of the fast mirror (X direction which corresponds to the lines acquisition). In the case of random mechanical movements, this noise is independent from one pixel to another, whereas in the case of the other defect the phase noise is present only between lines (no noise between pixel in the fast direction). Thus these two types of phase noise imply two different effects on final synthetic images. In our setup, random mechanical noise can be neglected and only the lack of repeatability in position of the fast mirror which produces around 0.1 radians of phase noise between lines of the images, can be considered (however the study is presented).

Theoretical analysis

We represent the random phase noise by a random function $\Phi(x,y)$ with the density function $P_\Phi(\phi)$. With this phase noise, the raw acquired wavefront $h_R(x,y)$ of Eq. (1) is turned into:

$$h_R^{PhN}(x,y) = m_{PhN}(x,y)h_R(x,y)$$
$$\mathrm{m}_{\mathrm{PhN}}(\mathrm{x},\ \mathrm{y}) = \exp(\mathrm{j}\ \Phi(x,y)) \tag{11}$$

In this expression m_{PhN} (x,y) is the dephasing term. Physically, h_R(x,y) corresponds to a wavefront generated by a waist r / √2 which has propagated over a distance L / 2, SA filtering corresponding to refocusing back this signal. When we introduce phase defects m_{PhN} (x,y) on the raw image, we simply generate speckle. Then the mean square of our signal (our final synthetic image is random as the phase noise function is random) is given by [17]:

$$\overline{\left|h_{SA}^{PhN}(x,y)\right|^2} \approx \left|h_{SA}(x,y)\right|^2 * \left(\left|\overline{\mathrm{m}_{\mathrm{PhN}}}(x,y)\right|^2 \delta(x,y) + (\frac{2}{\lambda L})^2 DSP_m(\frac{2x}{\lambda L},\frac{2y}{\lambda L})\right) \tag{12}$$

In this expression * is the convolution and $\overline{}$ the mathematical expectation operation. $DSP_m(\upsilon,\mu)$ is the power spectral density of m_{PhN} (x,y) – $\overline{m_{PhN}}$:

$$DSP_m(\upsilon,\mu) = FT(COV_m(x,y))$$
$$\overline{\mathrm{m}_{\mathrm{PhN}}} = \int_{-\infty}^{+\infty} \exp(\ j\phi) P_\Phi(\phi) d\phi = \tilde{P}_\Phi(1) \approx 1 - \frac{\sigma_\Phi^2}{2} \tag{13}$$

In this expression, COV_m(x,y) is the covariance of m(x,y) and $\tilde{P}_\Phi$ the characteristic function associated with random function Φ and σ_Φ its standard deviation. Eq. (12) shows that the SA operation divides the raw signal in two components: the first one is the signal we would have without any noise whereas the second one is the speckle term generated by the random phase noise on the raw signal. More precisely, the phase noise converts a part of the signal power into speckle, which is illustrated via the term $\overline{\left|m_{PhN}(x,y)\right|^2} = \left|\tilde{P}_\Phi(1)\right|^2 \approx \sigma_\Phi^2$ in Eq. (12) and (13); by conservation of the total energy from the raw signal, the proportion of the power in the speckle is

therefore 1 - $\left|\tilde{P}_{\Phi}(1)\right|^2 \approx 1 - \sigma_{\Phi}^2$. The greater the standard deviation of the random phase perturbation is, the higher the power conversion toward speckle is. More quantitatively, considering a Gaussian or a uniformly distributed phase noise we get:

- For the Gaussian noise:

$$\left|\overline{m_{PhN}(x,y)}\right|^2_{Gauss} = \left|\tilde{P}_{\Phi,Gauss}(1)\right|^2 = \exp(-\sigma_{\Phi}^2) \quad (14)$$

- For the uniform noise:

$$\left|\overline{m_{PhaseNoise}(x,y)}\right|^2_{Uni} = \left|\tilde{P}_{\Phi,Uni}(1)\right|^2 = \mathrm{sinc}^2\left(\frac{\sqrt{12}\sigma_{\Phi}}{2}\right) \quad (15)$$

Concerning the spatial features of the speckle contribution, we see from Eq. (12) and (13) that it depends on the covariance of m_{PhN}: the narrower the covariance is, the wider the speckle pattern is as we can see on Figure 6. If the phase noise is independent from one pixel to another (case of mechanical noisy movements), the width of the covariance of $\Phi(x,y)$ is directly equal to the size of one pixel δx and δy in X and Y directions respectively. More quantitatively, the width of $DSP_{mm}(x,y)$ is ~ 1 / δx in the X direction and so from Eq. (12) we deduce that the speckle pattern has a size ~ λ L / δx in X direction (size of a beam diffracted over a distance L through a hole of size δx). As a result at the minimum spatial sampling (Shannon limit: $\delta x \approx r$), the speckle has approximately the same size than the raw signal with a radius $RES_R(L)$.

Figure 6 here

In our case, as we said above, the phase noise is mainly due to a problem of malposition of the fast mirror, which creates a phase noise only along the slow direction Y (there is a slight shift between lines). As a result the speckle is created only along this slow direction. Because we have estimated this noise around $\sigma_\Phi \approx 0.1$ radian, we expect from Eq. (14) that only 1% of the raw signal power is sent toward speckle while 99% of the power is kept for the synthetic final image. This good performance is the reason why we have chosen galvanometric mirrors to create a translational movement between the target and the laser instead of simply moving the object with a mechanical translational stage. Despite these good performances, it is important to keep in mind that a phase noise of 2π (vibration amplitude of $\lambda/2$) is enough to totally convert our raw signal into speckle so phase noise remains a critical point that needs to be carefully handled.

As for the additive noise case, the SNR can be improved by filtering the speckle term of Eq. (12). Indeed, because it is spread in the whole Fourier space, the speckle can be reduced by spatial oversampling associated with an adapted filtering that preserves the useful signal. However, the power of the useful signal that has been converted into this speckle cannot be recovered.

Numerical verifications

An experimental validation of our theoretical predictions is delicate as we have shown that natural random vibrations are negligible. For those reasons, we have chosen to check the theory on simulated data. Figure 7 presents the effects of Gaussian random phase noise on SA final image:

Figure 7 here

We verify that in accordance to Eq. (12) and (13), when introducing phase noise into raw acquisition, the power in the synthetic image is transferred into speckle noise (Figure 7b and Figure 7c). When the phase noise σ_Φ exceeds π, the initial phase information is completely lost and all initial power in the raw image (Figure 7a) is turned into speckle (Figure 7d). We see on Figure 7c and Figure 7d that the width of the speckle pattern is close to the width of the raw signal (Figure 7a) which is consistent with the theoretical considerations (Figure 6).

Sinusoidal phase perturbations

We now focus on sinusoidal phase noise that arises for two reasons: the first one is the mechanical vibrations of the table and of all optical components which are generally at a low frequency (< 300 Hz). The second source of sinusoidal noise is the electric power supply: 50/60 Hz and its harmonics that can be present and impact the galvanometric mirror motors. Globally these perturbations have an amplitude between 0 and 0.5 radian depending on the quality of the setup (measure of the phase evolution when galvanometric mirrors are at rest) and the attention we have paid to the sources of vibration and to the electric shielding. As for the random phase noise, we discuss in the following the repercussion of this perturbation on the final synthetic image.

Theoretical analysis

Due to the scanning of the target, the sinusoidal temporal perturbation corresponds on the raw acquisition, to a spatial sinusoidal perturbation. Noting Φ_0 its amplitude and (υ_0, μ_0) its spatial frequency, the raw signal is now given by:

$$\begin{aligned} h_R^{SinPh}(x,y) &= m_{SinPh}(x,y)\,h_R(x,y) \\ m_{SinPh}(x,y) &= \exp(\,j\Phi_0 \sin(\,2\pi(\upsilon_0 x + \mu_0 y))) \end{aligned} \tag{16}$$

In this expression $m_{SinPh}(x,y)$ is the perturbation term. Once again, to easily explain the effects of this term on the final synthetic image, it is more convenient to make a physical interpretation: adding the perturbation $m_{SinPh}(x,y)$ is equivalent to insert a phase grating in front of the wavefront $h_R(x,y)$ before numerical refocusing (over a distance L /2). As a result, instead of having speckle, we now have several orders of diffraction and a repetition of several perfect synthetic images. Each of these images corresponds to an order of diffraction in our equivalent model of phase grating as illustrated on Figure 8. More precisely, the diffraction is along to the perturbation and the angles of diffraction are multiples of $\lambda\sqrt{\upsilon_0^2 + \mu_0^2}$ (see Figure 8). Because the SA filtering is equivalent to a retropropagation over a distance L / 2, the different orders are separated by a distance $\frac{\lambda L\sqrt{\upsilon_0^2 + \mu_0^2}}{2}$ on the final SA image:

$$h_{SA}^{SinPh}(x,y) = \sum_{n-\infty}^{+\infty} J_n(\Phi_0) h_{SA}(x - n\frac{\lambda\upsilon_0 L}{2}, y - n\frac{\lambda\mu_0 L}{2}) \qquad (17)$$

In this expression, $J_n(\Phi_0)$ is the Bessel function of order n. The proportion of the signal power sent in the order n is given by $\left|J_n(\Phi_0)\right|^2$. This expression is compatible with the total power conservation since $\sum_{n-\infty}^{+\infty}\left|J_n(\Phi_0)\right|^2 = 1$. As for random phase noise, the power of parasitic replicas (orders $\neq 0$) is taken on the signal of interest (order 0).

Figure 8 here

In contrast to the previous perturbations (additive and random phase noises), oversampling and adapted filtering cannot reduce the image doubling effects.

Experimentally, we observe a vibration amplitude between 0 and 0.5 radian. According to Eq. (17), this corresponds to a transfer around 10% from order 0 (image we would get without noise) toward higher orders (parasitic replicas). As it was the case for random phase noise, an amplitude Φ_0 around π is enough to completely loose the phase information and the order 0 so it is very important to limit all sources of vibration and electric noise.

Experimental verification

To experimentally check the effects of the sinusoidal phase noise, we recorded a raw image (with a defocus of 2.5 cm) of the object of Figure 2 with or without imposing a mechanical vibration during acquisition. This vibration is imposed by an external loud speaker @ 100 Hz with an integration time T = 150 μs and a spatial sampling of 1.7 μm by pixel. Experimentally this creates a spatial frequency $\upsilon_0 \approx 10000$ m^{-1} in the rapid direction (X). In the other direction (Y) we have measured $\mu_0 \approx 80000$ m^{-1}. The SA operation is then applied to recover the resolution. Synthetic amplitude images are presented on Figure 9:

Figure 9 here

Image replicas corresponding to diffraction orders can be observed on Figure 9 (here we see orders -1, 0 and 1). In theory, from Eq. (17) we expect a shift of $\lambda\upsilon_0 L/2 = 130$ μm and $\lambda\mu_0 L/2 =$ 1.1 mm in X and Y directions respectively, what is conform to our experimental synthetic image on Figure 9b. Moreover, we have verified that the power distribution in different orders is given by Eq. (17).

Phase drifts

There is a last possible phase perturbation: slow phase drift (compared to fast direction). This drift is mainly due to temperature fluctuations in the laser crystal when we turn on the laser or the fluctuations of the pump laser diode. Another important cause is the variations of the optical path between the laser and the target due to slight variation of the refractive index of the air (because of temperature or pressure changes). As a result, this phase drift can be highly reduced by isolating the system from atmospheric changes but it is difficult to completely eliminate it. In our case, the phase drift is around π radians/minute. In the following we present the impact of this phase drift on the final synthetic image.

Theoretical analysis

Considering this perturbation, the raw signal can now be written as:

$$\begin{aligned} h_R^{PhDrift}(x,y) &= m_{PhDrift}(y)\, h_R(x,y) \\ \mathrm{m}_{\mathrm{PhDrift}}(\mathrm{y}) &= \exp(\mathrm{j}\ \Phi(y)) \end{aligned} \tag{18}$$

We can see that the phase perturbation depends only on the Y coordinate which is the slow direction. This can be explained by the fact that we consider the case of a slow phase drift. As for the two previous phase perturbations, we propose a physical analogy: instead of a ground glass (random phase) or a grating (sinusoidal noise) in front of equivalent wavefront, the slow phase drift introduces optical aberrations. As a result, the final synthetic image is distorted along the Y direction only, depending on the precise aberrations which have been introduced. More quantitatively, as it is the case for the two previous phase noises, one part of the power in the center of the synthetic PSF (Eq. (3)) is lost proportionally to σ_Φ^2 (variance of the aberration) and transferred into adjacent pixels which enlarges this synthetic image. Thanks to this ascertainment, we see that a drift of 2π is enough to highly degrade the final synthetic image.

Then because in our case the acquisition time is around one minute and the phase drift is around π radians/minute, this phase perturbation is very critical and needs to be corrected. Instead of making only one acquisition with a fast scan along the X direction leading to Eq. (18) but which results in degradation along the Y direction, we propose to make a second acquisition but with a fast scan along Y. We then have two images: one without drift along X and the other along Y, but by combining them we recover a corrected "raw" acquisition before applying SA filtering and getting an aberration-free synthetic image.

Experimental verification

To experimentally illustrate our theoretical considerations we acquired two raw images (one with a fast acquisition along the X and the other along the Y direction) of the object of Figure 2 with a defocus L = 2 cm with a high phase drift. The phase drift is accentuated by an external perturbation of the laser diode (which pumps the laser crystal) power supply in order to have a phase variation of more than π over a length RES_{SA} (that is to have significant impact on the final synthetic image, see Eq. (3)). The results are shown in Figure 10:

Figure 10 here

Figure 10e shows the amplitude of synthetic image from one of the two raw acquisitions (precisely when Y is the slow direction, Figure 10a is its amplitude and Figure 10b its phase). We verify that in accordance to the theory, the phase drift causes vertical aberrations. Figure 10c is the phase difference between the two images before any correction; we see there is a phase drift in both directions because of the two different slow directions used during acquisition. By using this image we can correct the first raw image (with drift along Y) by eliminating vertical phase difference between the two images. This phase correction to apply is of course independent from the column and so Figure 10c is averaged along X (Figure 10d). Finally when

SA operation is applied to the corrected image, we get Figure 10f which is free of aberration, showing the efficiency of our correction method.

5) Conclusion and perspectives

This paper is a continuation of [14] where we presented a Synthetic Aperture LOFI-based setup for in-depth imaging through scattering media. We have studied the main sources of noise that can impact the acquisition, their repercussion on final synthetic images and proposed solutions to limit their influence. More precisely we have divided noises into two families: additive (amplitude) noise and multiplicative (phase) noise. The first one is due to shot noise and can be reduced (relatively to the power SNR) proportionally to the global time measurement by increasing the integration time per pixel T, or by oversampling image during acquisition and use adapted filtering. The second one can itself be divided into three sub-families: random phase noise, mainly caused by galvanometric mirror malposition from one line to another, sinusoidal phase noise due to mechanical vibrations and phase drifts caused by slow variations of temperature and pressure in the setup. Because they are multiplicative noises, they all convert a power fraction $1 - \sigma_\Phi^2$ (σ_Φ is the mean noisy phase excursions) of the signal (useful signal and parasitic reflections) into parasitic signal which depends on the precise nature of the perturbation. This noise is pretty low but it is important to keep in mind that $\sigma_\Phi \sim \pi$ can be sufficient to completely destroy the phase information. That is why phase noise can be catastrophic if not controlled. Concerning random phase noise, this parasitic signal can be compared to speckle and can be partially reduced by oversampling and adapted filtering (as for amplitude noise). Sinusoidal phase noise is like introducing a grating which splits the useful signal in several orders each order corresponds to an image replica. Finally, phase drifts lead to aberrations in the direction of slow acquisition which can be corrected by combining two images with different

“slow directions”. The study we made in this paper is related to our previous work [14,15] but can easily be generalized to all interferometric imaging systems and especially those with a raw acquisition which is made point by point. This is the case for most of other SA systems in the radar [18,19], optical [20,21] or more recently Terahertz domain [22].

To conclude, beside the signal a large amount of noise sources need to be limited: specular (can be filtered because it is constant) and diffusive parasitic reflections [15], shot noise, and noise converted from signal (useful and parasitic reflections) to “speckle” by phase noise. In order to make images through scattering media, the main challenge is to realize images with minimum number of photons. In this case, “speckle” converted from useful signal by phase noise can be neglected but we see that close to the ultimate limit (shot noise), noise due to parasitic reflection is still present (diffusive or/and specular associated to the phase noises). A solution proposed in [23] consists in tagging photons with an acoustic transducer just in front of the target in order to eliminate parasitic reflections from the signal. Unfortunately the proposed setup gives only access to the amplitude of the reinjected signal. Future work will de dedicated to adapt it in order to recover the phase which is needed for Synthetic Aperture operations.

REFERENCES

1. S. M. Popoff, G. Lerosey, R. Carminati, M. Fink, A. C. Boccara, and S. Gigan, "Measuring the Transmission Matrix in Optics : An Approach to the Study and Control of Light Propagation in Disordered Media," Phys. Rev. Lett. **104**, 100601 (2010).
2. M. Pernot, J-F. Aubry, M. Tanter, A-L Boch, F. Marquet, M. Kujas, D. Seilhean, and M. Fink, "In vivo transcranial brain surgery with an ultrasonic time reversal mirror," J. Neurosurg. **106**, 1061-1066 (2007).
3. I. M. Vellekoop, C. M. Aegerter, "Scattered light fluorescence microscopy : imaging through turbid layers," Opt. Letter. **35**, 1245-1247 (2010).
4. A. Dubois, C. Boccara, "Full-filed OCT," M S-Medecine Sciences. **22**, 859-864 (2006).
5. P. Pantazis, J. Maloney, D. Wu, S. E. Fraser, "Second harmonic generating (SHG) nanoprobes for in vivo imaging," PNASUSA. **107**, 14535-14540 (2010).
6. M. Minsky, "Memoir on inventing the confocal scanning microscope," Scanning. **10**, 128-138 (1988).
7. S. Vertu, J. Flugge, J.J. Delaunay, and O. Haeberle, "Improved and isotropic resolution in tomographic driffractive microscopy combining sample and illumination rotation," CENTRAL EUROPEAN JOURNAL OF PHYSICS. **44**, 969-974 (2011).
8. E. Lacot, R. Day, and F. Stoeckel, "Coherent laser detection by frequency-shifted optical feedback," Phys. Rev. A **64**, 043815 (2001).
9. K. Otsuka, "Self-Mixing Thin-Slice Solid-State Laser Metrology," Sensors. **11**, 2195-2245 (2011).
10. E. Lacot, R. Day, and F. Stoeckel, "Laser optical feedback tomography," Opt. Letters. **24**, 744-746 (1999).

11. O. Hugon, F. Joud, E. Lacot, O. Jacquin, and H. Guillet de Chatellus, "Coherent microscopy by laser optical feedback imaging (LOFI) technique," Ultramicroscopy. **111**, 1557-1563 (2011).
12. E. Lacot, O. Jacquin, G. Roussely, O. Hugon, and H. Guillet de Chatellus, "Comparative study of autodyne and heterodyne laser interferometry for imaging," J. Opt. Soc. Am. A **27**, 2450-2458 (2010).
13. O. Jacquin, E. Lacot, W. Glastre, O. Hugon, and H. Guillet de Chatellus, "Experimental comparison of autodyne and heterodyne laser interferometry using Nd:YVO4 microchip laser," J. Opt. Soc. Am. A **28**, 1741-1746 (2011).
14. W. Glastre, O. Jacquin, O. Hugon, H. Guillet de Chatellus, and E. Lacot, "Synthetic aperture laser optical feedback imaging using a translational scanning with galvanometric mirrors, " J. Opt. Soc. Am. A, doc. ID 163929 (posted 29 February 2012, in press). (Available on HAL & Arxiv)
15. W. Glastre, E. Lacot, O. Jacquin, and H. Guillet de Chatellus, "Sensitivity of synthetic aperture laser optical feedback imaging, " J. Opt. Soc. Am. A. **29**, 476-485 (2012).
16. A. Witomski, E. Lacot, O. Hugon, and O. Jacquin, "Two dimensional synthetic aperture laser optical feedback imaging using galvanometric scanning," Appl. Opt. **47**, 860–869 (2008).
17. J. W. Goodman, *Speckle Phenomena in Optics* (Roberts and Company Publishers, 2006).
18. J. C. Curlander and R. N. McDonough, Synthetic Aperture Radar: Systems and Signal Processing, (Wiley, 1991).
19. A. Ja. Pasmurov and J. S. Zimoview, *Radar Imaging and Holography*, (Institution of Electrical Engineers, 2005).

20. C.C. Aleksoff, J.S. Accetta, L.M. Peterson, A.M.Tai, A.Klossler, K. S. Schroeder, R. M. Majwski, J. O. Abshier, and M. Fee, "Synthetic aperture imaging with a pulsed CO2 laser," Proc. SPIE **783**, 29–40 (1987).
21. S. Markus, B. D. Colella, and T. J. Green, Jr., "Solid-state laser synthetic aperture radar, " Appl. Opt. **33**, 960 – 964 (1994).
22. A. Bandyopadhyay, A. Stepanov, B. Schulkin, M. D. Federici, A. Sengupta, D. Gary, and J. F. Federici, "Terahertz interferometric and synthetic aperture imaging, " J. Opt. Soc. Am. A. **23**, 1168-1178 (2005).
23. O. Jacquin, W. Glastre, E. Lacot, O. Hugon, H. Guillet de Chatellus, and F. Ramaz, "Acousto-optic laser optical feedback imaging, " Opt. Letters. **37**, 2514-2516 (2012).

FIGURE CAPTION

Figure 1: Experimental setup of the synthetic aperture LOFI-based imaging system. The laser is a cw Nd:YVO_4 microchip collimated by lens L_1. A beam splitter sends 10% of the beam on a photodiode connected to a lock-in amplifier which gives access to the amplitude and phase of the signal. The frequency shifter is made of two acousto-optic modulators which diffract respectively in orders 1 and -1 and give a net frequency shift of $F_e / 2 = 1.5$ MHz. X-Y plane is scanned by galvanometric mirrors M_X (scan in the X direction) and M_Y (scan in the Y direction) conjugated by a telescope made by two identical lenses L_3. f_3 and f_4 are the focal lengths of L_3 and L_4. α_X and α_Y are the angular positions of M_X and M_Y. r is the waist of the laser after L_4.

Figure 2: Target used for the whole study: it is made of reflective silica beads of 40 μm diameter behind a circular aperture of 1 mm diameter. The bright field transmission image is made through a Zeiss microscope objective with a magnification of 10 and a 0.25 numerical aperture (focal length of 20 mm).

Figure 3: Illustration of the effect of the spatial sampling on the Fourier content of the signal. The images are the amplitude of the Fourier transform of a simulated PSF with the following parameters: r = 20 μm, f = 75 mm and L = 2.5 cm. For a constant field image of 2 mm, we have a sampling of a) 128*128 pixels and b) 1024*1024 pixels.

Figure 4: Amplitude of SA images of the setup of Figure 2. Parameters are r = 20 μm, f = 75 mm and L = 2.5 cm. Images a), c) show a sampling of 128*128 pixels and b), d) a sampling of 1024*1024 pixels. Figures are amplitude images after filtering a), b) by phase filter of Eq. (4) and c), d) adapted filter of Eq. (8).

Figure 5: Dependence of the power in a pixel of signal and noise (averaged) in the SA image with the acquisition time. The signal comes from the object of Figure 2 with parameters r = 20 μm, f = 75 mm and L = 2.3 cm. Acquisition time is increased via a) the integration time in a pixel at constant sampling and field of view or b) the sampling at constant integration time T and field of view. The power here is the mean of the square of the image amplitude. This power is normalized by the total number of pixels. The noise is measured in the absence of beads (see Figure 4).

Figure 6: Propagation of a wavefront with phase noise over a distance L/2. In the final image plane we have two contributions: a coherent one (plain line) and a random speckle (dashed line). The speckle and coherent contributions have relative intensities depending only on the density of probability of the random phase.

Figure 7: Effect of random Gaussian phase noise on SA operation. We use a simulated image of a punctual reflector. a) Amplitude of raw image with L = 4 cm, b) Amplitude after numerical refocusing, without phase noise, c) Amplitude after numerical refocusing, $\sigma_\Phi = 3\pi/5$ and d) Amplitude after numerical refocusing, $\sigma_\Phi = \pi$. Parameters are r = 20 μm, f = 75 mm and the definition is 512*512 pixels; the numerical refocusing is made with the pure phase filter for all images.

Figure 8: Propagation of a wavefront with sinusoidal phase perturbations over a distance L/2. In the final image plane, there are two contributions: a coherent one (plain line) and several diffracted orders (dashed line). υ_0 and μ_0 are spatial frequencies of the perturbation in X and Y directions; the drawing is a projection along to the sinusoidal perturbation.

Figure 9: Effect of a mechanical sinusoidal phase perturbation on SA operation. Image parameters are 2048*2048 pixels, L = 2.5 cm, r = 20 μm, f = 75 mm, integration time T = 150 μs by pixel and the target is the object of Figure 2. Amplitude image after synthetic aperture operation a) without and b) with the perturbation. The perturbation at 100 Hz is generated by a loud speaker localized near the target. This induces a phase perturbation of amplitude $\Phi_0 = 1.2$ radian and of spatial frequencies $\upsilon_0 = 10000$ m^{-1} and $\mu_0 = 80000$ m^{-1}. The SA operation is made with the pure phase filter of Eq. (4).

Figure 10: Effect of phase drifts during the raw acquisition on SA imaging. Parameters are r = 13 µm, f = 25 mm, L = 2 cm and 512*512 pixels. The effect of the phase drift correction is illustrated too (here the correction is made on the image taken slowly along Y direction). The target is still the object of Figure 2. a) Amplitude and b) phase (white is -π radians and the black is +π) of raw image of the target. Image c) shows phase difference between the two raw acquisitions acquired with different slow directions. d) is the phase correction to apply in the Y direction calculated from c). The last two images are the amplitudes of the synthetic image (pure phase filter is used) e) before and f) after phase correction.

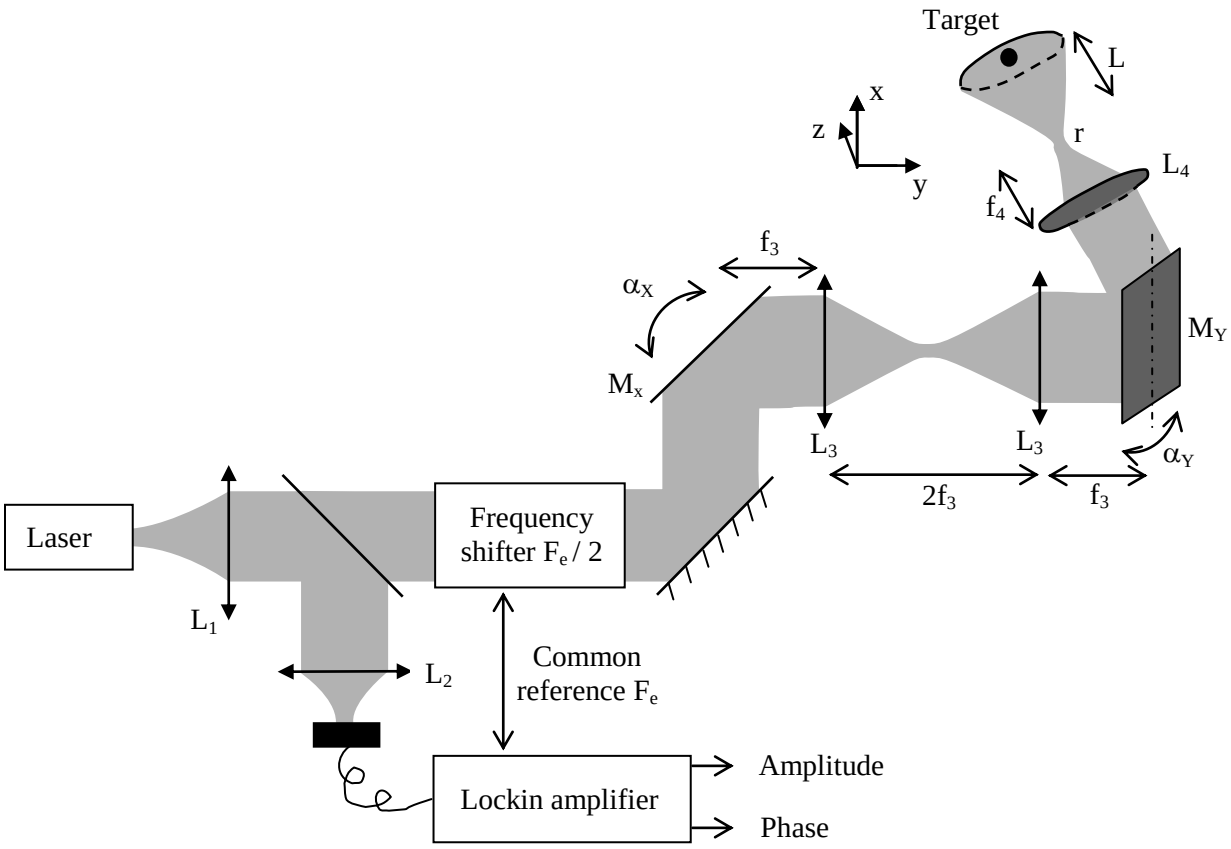

Figure 1

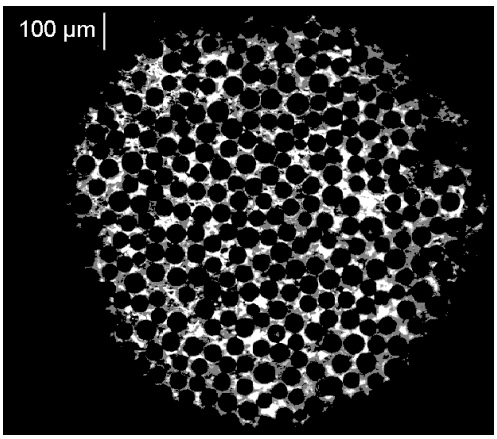

Figure 2

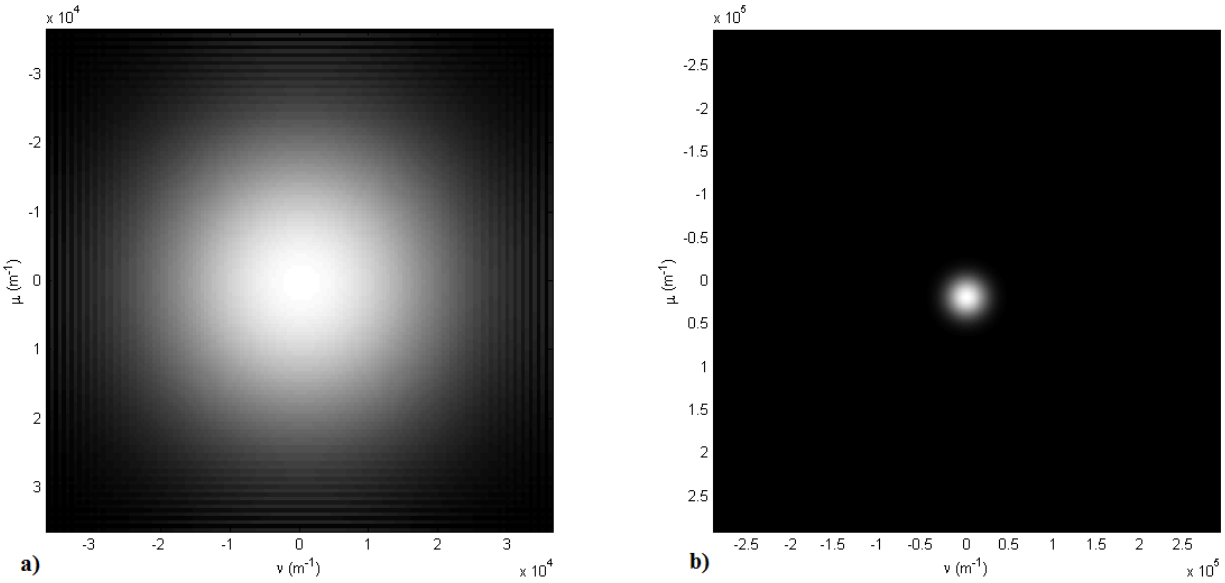

Figure 3

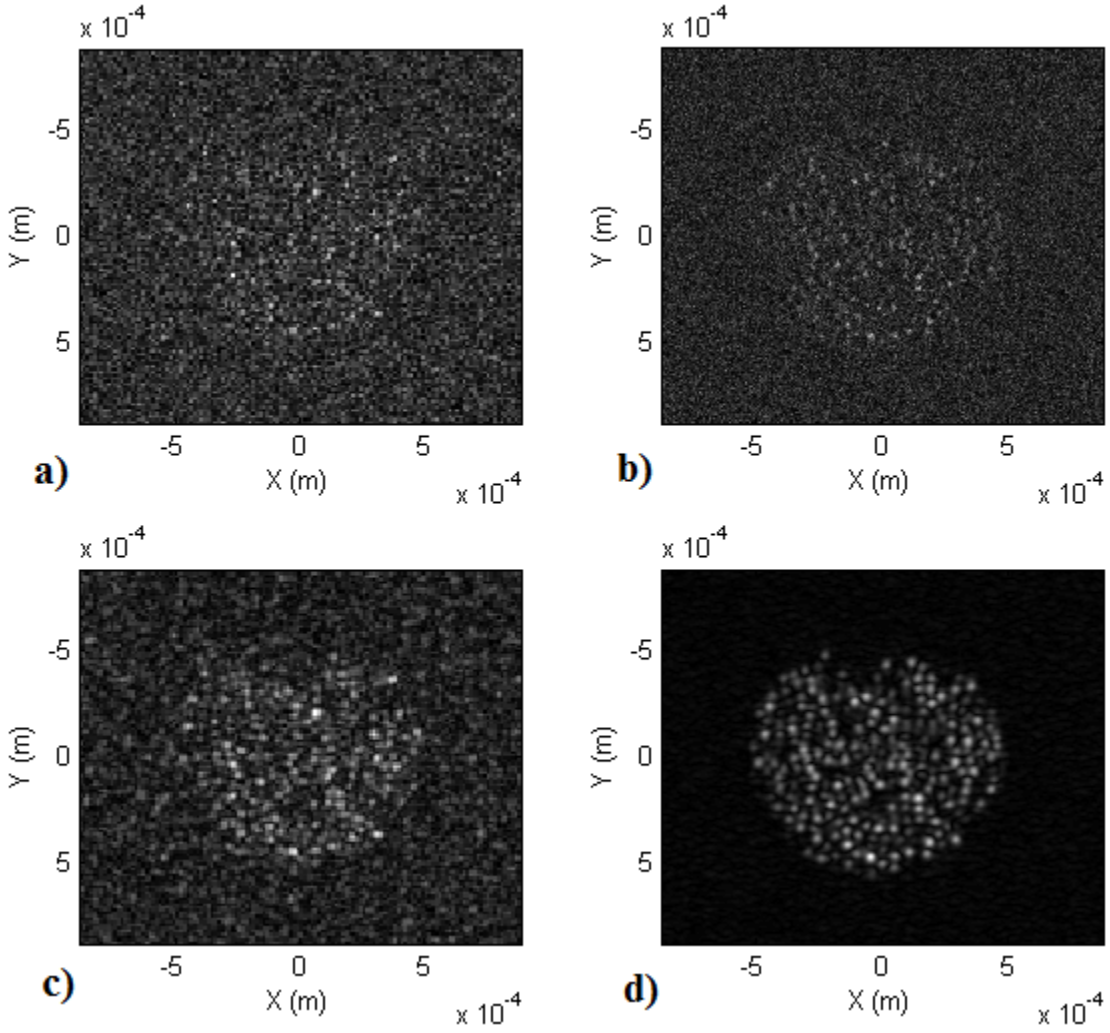

Figure 4

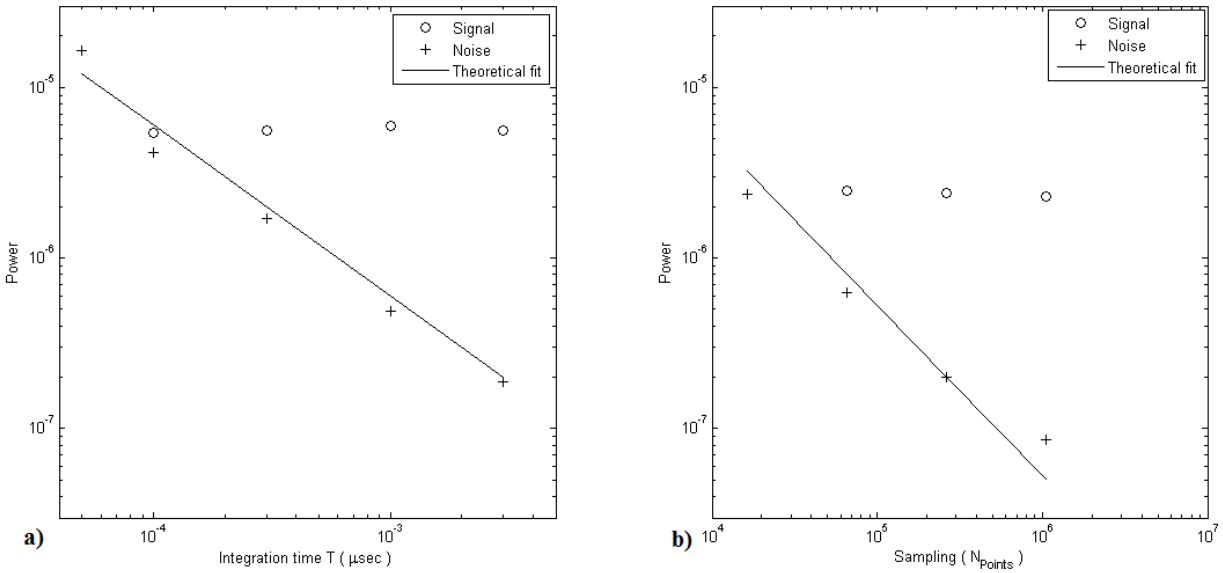

Figure 5

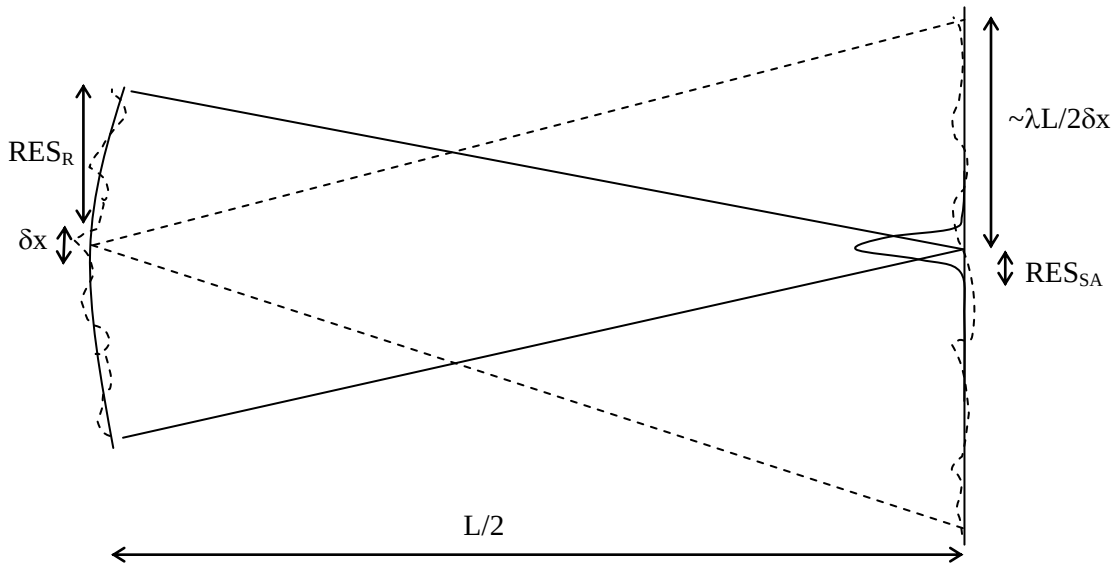

Figure 6

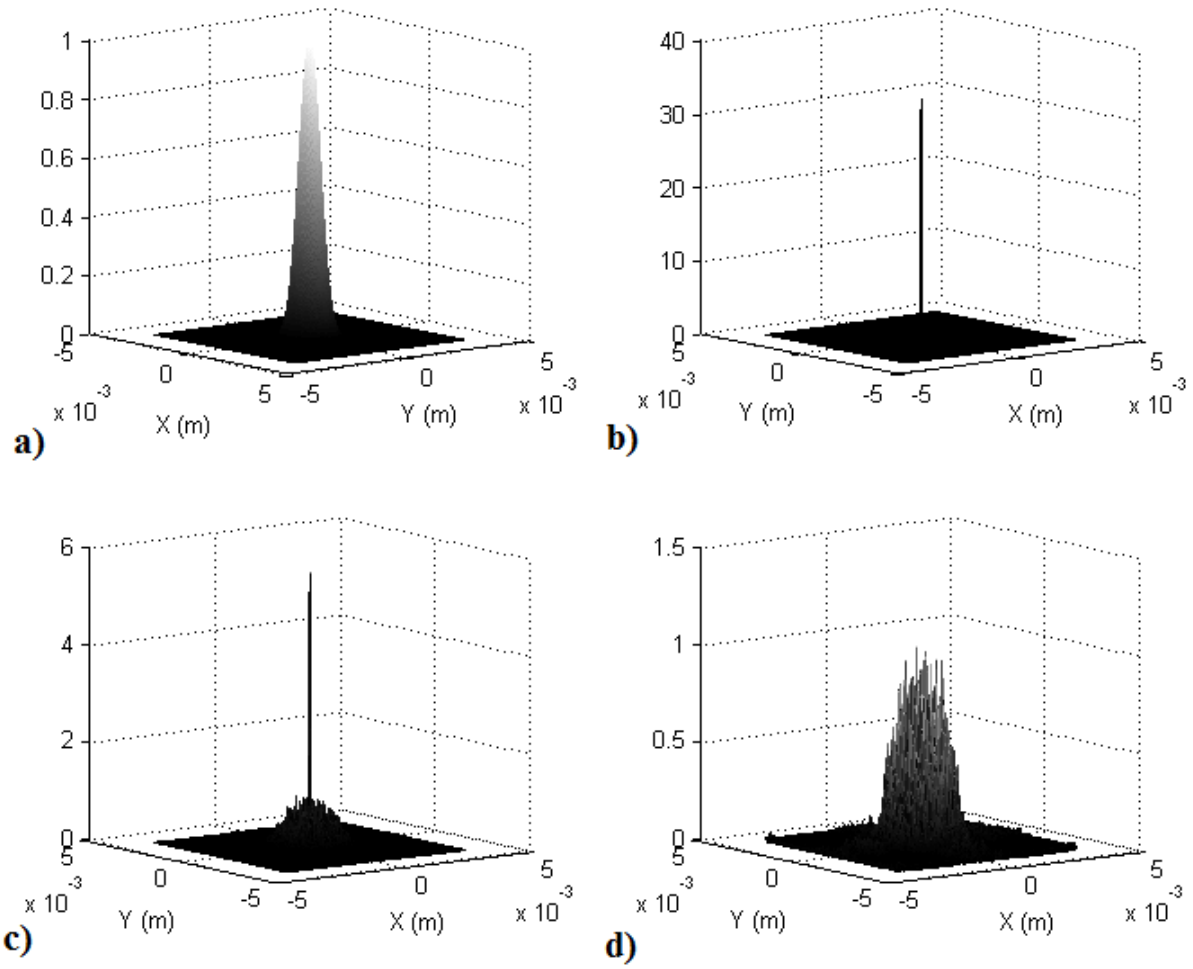

Figure 7

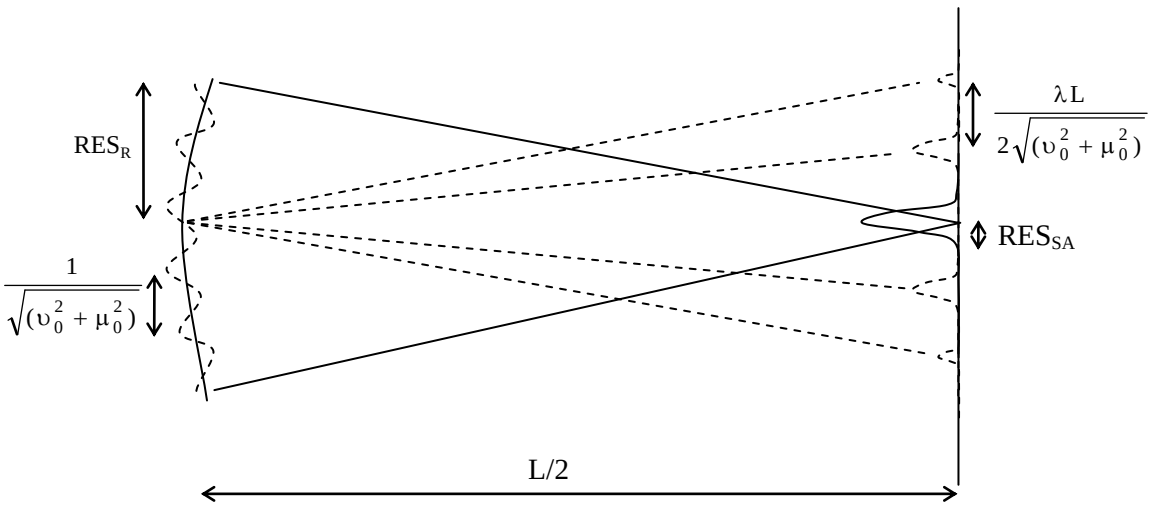

Figure 8

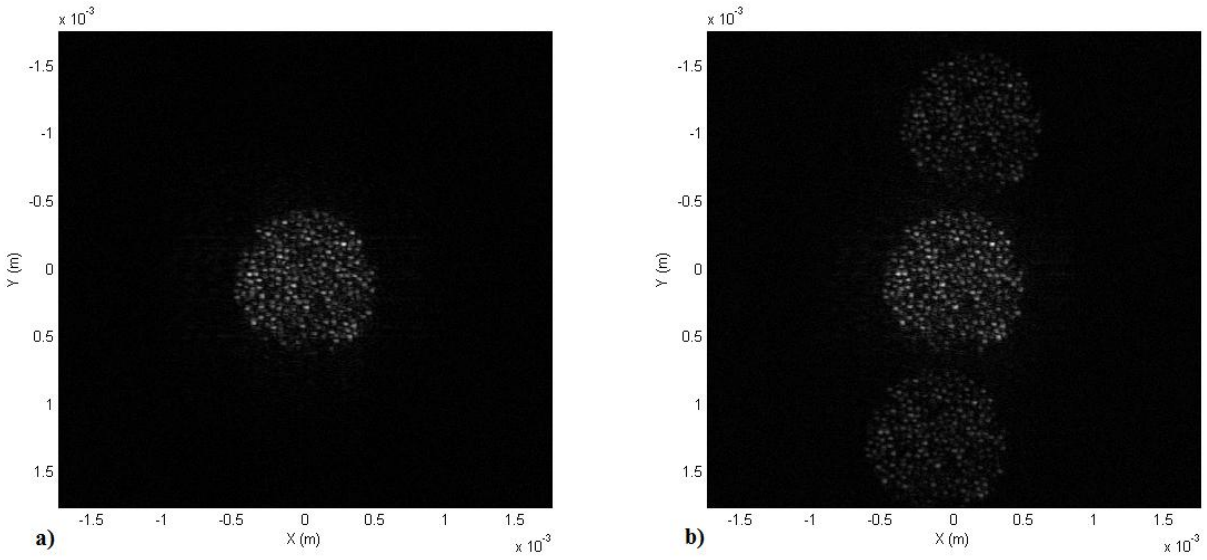

Figure 9

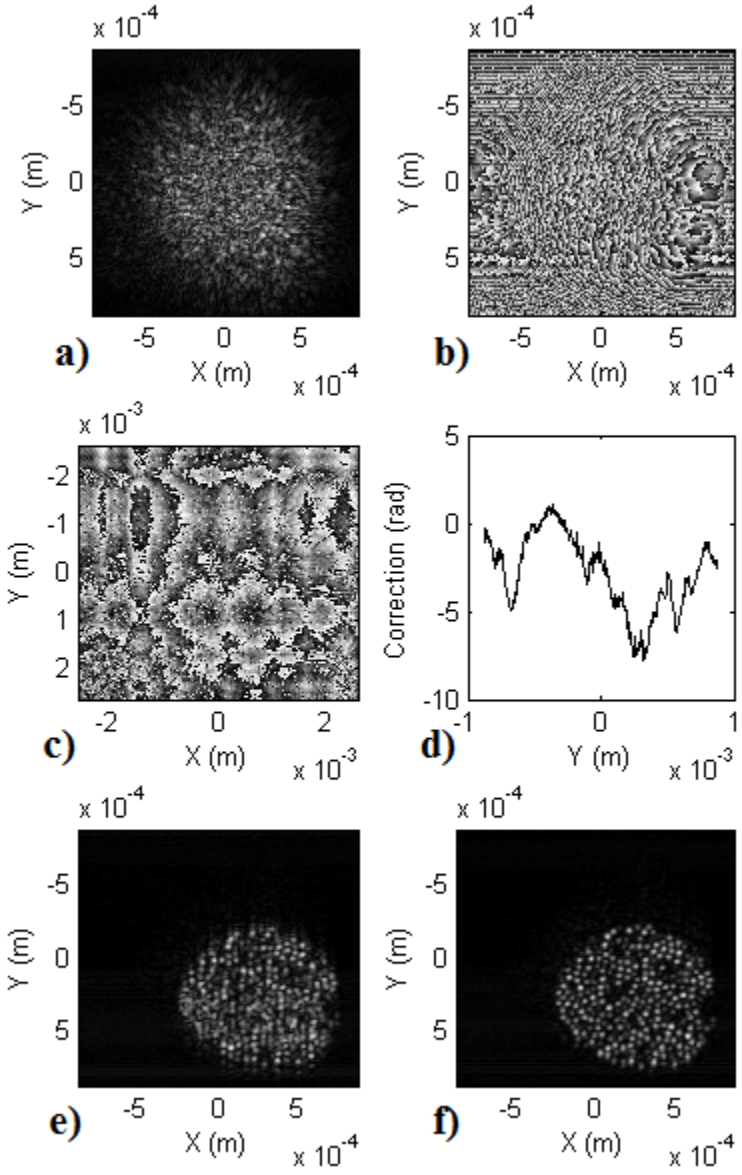

Figure 10